RESEARCH ARTICLE

BON VIEW PUBLISHING

Theoretical Studies on γ-Photon/Neutron Shielding Characteristics of RE³⁺ Co-doped Borate, Phosphate, and Silicate Glass Systems

Murugasen Priya[1,*] , **A. Antony Suresh**[1], **M. Dhavamurthy**[2] **and A. V. Deepa**[3]

[1]*Department of Physics, Saveetha Engineering College, India*

[2]*Department of Physics, Mannai Rajagopalaswamy Government Arts College, India*

[3]*Department of Physics, Mohammed Ali Shihab Thangal Memorial Arts & Science College, India*

Abstract: The Phy-X program software was used to investigate the γ and neutron shielding properties of trivalent rare earth co-doped borate, phosphate, and silicate glasses (G1–G10) concerning elemental composition and density. The attenuation coefficients (μ/ρ and μ), half/tenth-value layer (HVL and TVL), and mean free path were calculated, and each revealed the influence of rare earth including the Pb, Ba, and Bi elements. Energy and compositional dependent effective atomic number, effective electron density (N_{eff}), and effective electron conductivity (C_{eff}) of all the glasses were studied. On the high-density glasses G6, G9, and G10, the HVL and TVL values are projected to be lower than on the other examined glasses. The neutron radiation shielding abilities of the studied glasses were investigated by determining removal cross-section. The results were compared to those of commercially available materials such as concrete, graphite, water, and Hematite-serpentine concrete. The γ-ray exposure buildup and energy absorption factor values of glass samples were determined in the energy range of 0.015 to 15 MeV.

Keywords: co-doped rare-earth (RE)-shielding glasses, attenuation coefficient, equivalent atomic number (Z_{eq}), buildup factors, penetration depth

1. Introduction

Radiation is now applied in a wide range of disciplines, including nuclear power plants, diagnostics in medicine, and agriculture. The shielding material should possess special qualities that enable it to effectively attenuate damaging radiation. The shielding effectiveness of materials can be evaluated using various parameters including linear attenuation coefficient (LAC) (μ), mass attenuation coefficient (μ/ρ), HVL, and TVL. The HVL, TVL, and mean free path (MFP) are all characteristics that can be used to indicate the penetration thickness of a material. These are essential considerations when comparing the thickness of two or more materials. The effective atomic number (Z_{eff}) is a measure for visualizing photon interactions with multi-elemental materials based on atomic number. The Z_{eff} and effective electron density (N_{eff}) are essential variables in various applications, such as measuring absorbed dosage, modeling radiation shielding, exposure, and energy absorption buildup factors. The γ-ray buildup factors, namely the exposure buildup factor (EBF) and the energy absorption buildup factor (EABF) are multiplicative factors used to incorporate scattered photons' contribution into the normalized response to un-collided photons. The above variables can provide valuable information about how the radiation interacts with the attenuating substance.

Lead (Pb) and concrete are currently the most conventionally used radiation shielding materials; however, both have drawbacks. Pure Pb bricks are quite opaque and poisonous, and the density of concrete diminishes over time [1, 2]. Several theoretical and experimental studies were conducted to investigate new materials that could replace Pb in various radiation shielding applications. Glass materials have long been considered to be a viable concrete alternative. Glasses are attracting researchers nowadays due to their visual transparency as well as their potential capabilities in attenuating ionizing radiations. There are numerous studies on the qualities of γ-ray and neutrons shielding of various glass systems. Borate, germinate-tellurite, phosphate, and tellurite glasses doped with metal oxides such as barium oxide (BaO), sodium oxide (Na₂O), and erbium oxide (Er₂O₃) show excellent optical properties, thermal stability, and a high shielding performance with good transparency.

There are numerous studies on various glass systems and their qualities of γ-ray shielding in the literature. Kirdsiri et al. [3] calculated the mass attenuation coefficient (MAC) (μ/ρ) value for silicate glasses which included BaO, PbO, and Bi₂O₃. According to these authors, the increase of PbO and Bi₂O₃ concentration improved the μ/ρ. The increasing B₂O₃ concentration in the telluride Pb glass system increases Z_{eff} while decreasing the mass attenuation coefficient and mass removal cross-section [2]. Vani et al. [4] reported that the fluoro tellurite glass system doped with heavy metals such as barium can increase shielding features and replace Pb-based glasses and concrete.

*****Corresponding author:** Murugasen Priya, Department of Physics, Saveetha Engineering College, India. Email: priyam@saveetha.ac.in

In general, the desired shielding glass must have higher Z_{eff} and mass/LAC values, as well as minimum irradiation impacts on structural, optical, and mechanical properties. Phosphate (P_2O_5) and borate (BO_3) are two examples of stimulating hosts that are often utilized. The essential advantage of phosphate over other oxide glasses like borate and silicate is its ability to remain amorphous while also hosting high concentrations of transition metal ions. Furthermore, phosphate glasses have several desirable features that make them suitable for achromatizing borate flint glasses, including high solubility of RE^{3+} ions, high thermal stability, low melting point, and outstanding transparency. Because of optical uniformity, engineering structuring ease of fabrication, and stability in dopant concentration, glasses are the best host resources for RE^{3+} doping among the numerous host resources.

Rare earth element dopants in glasses help in improving their densities along with the densities, thermal characteristics, and network structure. However, the radiation shielding capabilities of rare earth-doped (especially co-doped) glasses have not been well investigated. A few reports have been published on the use of rare earth-doped glasses for shielding applications, some of which are listed below. Naseer and Marimuthu [5] evaluated the capacity of ytterbium and erbium co-doped bismuth (Bi) boro-phosphate glasses with various concentrations of Yb^{3+} to shield against γ-radiations and found that increasing the Yb_2O_3 in affects the shielding factors of glass. Mhareb [6] studied Er^{3+}/Sm^{3+} in Li_2O-B_2O_3-MgO-Er_2O_3-Sm_2O_3 glasses and found that the photon/neutron shielding properties were improved as the Sm^{3+} content increased. Kaur et al. [7] prepared Sm^{3+}/Gd^{3+} co-doped Pb aluminophosphate glasses and examined their prospect as high-energy radiation sensing and shielding. Rammah et al. [8] investigated the radiation shielding properties of Eu^{3+} boro tellurite glass.

Bi is a low-toxicity alternative to Pb in many industries. Due to the environmental hazards of Pb and protectionism in the global economy, Bi and barium are increasingly being used to substitute Pb in radiation glass shielding [9]. Sallam et al. [10] investigated the shielding parameters of Bi borate glasses doped transition metals, the glass possesses high density, high refractive index, and high optical basicity. The inclusion of transition metal oxides in the system absorbs the electrons from the irradiation source and is expected to enhance the shielding performance of the glass. Among the alkaline earth oxides (i.e., BaO, CaO, SrO, and MgO), BaO possesses the largest density, has a high Z_{eff}, and is a non-toxic compound. Chanthima et al. [11] found that BaO-doped glasses have a higher shielding efficiency than typical concretes such as hematite serpentine, basalt-magnetite, and limonite-limonite. Kaur et al. [12] investigated the physical parameters of the Bi borate glass system (Bi_2O_3-BaO-B_2O_3) modified barium and discovered that adding Ba increases the Z_{eff} while lowering the MFP and TVL.

The study examines the shielding ability of the rare earth (RE) co-doped borate-, phosphate-, and silicate glasses, as well as the effect of rare earth and heavy metals (Ba, Pb, and Bi) in these glasses on shielding applications. The attenuation coefficients, penetration depth, Z_{eff}, N_{eff}, and equivalent atomic number of glass samples were studied with exposure buildup factor (EBF) and EABF. According to our findings, Ce^{3+}/Tb^{3+} co-doped germanate–borate–silicate (GBS) scintillating glass (G6), and Pr^{3+}/Nd^{3+} co-doped alumina boro-phosphate (G5) glasses are excellent in radiation shielding. This research should be highly valuable in many applications of these glasses for radiation shielding efficacy in nuclear reactor core design and other sectors.

2. Theoretical Framework

Phy-X/PSD software[1] is a user-friendly online software and was used to compute all the relevant shielding parameters using the density and molar concentration of composition in the following rare earth co-doped borate, phosphate, and silicate glasses. The glass composition and the density is an essential quantity in radiation shielding materials, and it is directly related to the μ/ρ, HVL, and MFP values of G1 to G10 glasses are listed in Table 1. In general, the higher the radiation shielding characteristics of

Table 1
Glass notion, weight percentage of the elemental compositions, and density of the studied glasses

Sample code	Sample Name and Elements compositions	Density (g/cm³)	Ref. No.
G1	**Ce^{3+}/Dy^{3+} co-doped alumina boro-phosphate glass**	3.129	[13]
	40 H_3BO_4 + 49 H_6NO_4P + 10 Al_2O_3 + 0.5 CeO_2 + 0.5 Dy_2O_3		
G2	**Ce^{3+}/Sm^{3+} co-doped alumina boro-phosphate glass**	3.096	[13]
	40 H_3BO_4 + 49 H_6NO_4P + 10 Al_2O_3 + 0.5 CeO_2 + 0.5 Sm_2O_3		
G3	**Ce^{3+}/Dy^{3+} co-doped alumina-barium borate glass**	3.381	[14]
	60 B_2O_3 + 28 $BaCO_3$ + 10 Al_2O_3 + 1 Ce_2O_3 + 1 Dy_2O_3		
G4	**Ce^{3+}/Sm^{3+} co-doped alumina-barium borate glass**	3.342	[14]
	60 B_2O_3 + 28 $BaCO_3$ +10 Al_2O_3 + 1 Ce_2O_3 + 1 Sm_2O_3		
G5	**Pr^{3+}/Nd^{3+} co-doped alumina boro-phosphate glass**	3.118	[14]
	40 H_3BO_4 + 49 H_6NO_4P + 10 Al_2O_3 + 0.5 PrO_2 + 0.5 Nd_2O_3		
G6	**Ce^{3+}/Tb^{3+} co-doped GBS scintillating glass**	4.796	[15]
	25.3 SiO_2 + 24 B_2O_3 + 3 BaO +9 Al_2O_3 + 30 Gd_2O_3 + 3 P_2O_5 +5 Tb_2O_3 + 0.2 Ce_2O_3 + 0.5 Sb_2O_3		
G7	**Dy^{3+}/Pr^{3+} co-doped lithium borate glass**	2.430	[16]
G8	27.5 Li_2O + 71.7 B_2O_3 + 0.5 Dy_2O_3 + 0.3 Pr_6O_{11}	2.581	
	27.5 Li_2O + 71.3 B_2O_3 + 0.5 Dy_2O_3 + 0.7 Pr_6O_{11}		
G9	**Eu^{3+}/Nd^{3+} co-doped silicate glass**	3.807	[17]
G10	45 SiO_2 + 20 K_2O + 5 Na_2O + 16 PbF_2 + 10 LiF + 1 Eu_2O_3 + 3 Nd_2O_3	3.789	
	45 SiO_2 + 20 K_2O + 5 Na_2O + 18 PbF_2 + 10 LiF +1 Eu_2O_3 + 1 Nd_2O_3		

[1]Available at https://phy-x.net/PSD

glass, the more electrons and atoms per unit volume of the material that can interact with γ-photons/neutrons. Table 1 outlines the molar fraction of various types of rare earths co-doped with the host glass composition.

3. Shielding Parameters

3.1. Mass and linear attenuation coefficient

γ-ray photons with intensity I_o penetrate a layer of materials with density ρ and thickness t, resulting in intensity I determined by the Beer-Lambert law:

$$\frac{I}{I_o} = \exp\left[-\left(\frac{\mu}{\rho}\right)t\right] \tag{1}$$

Rearrange the above equation to get the mass attenuation coefficient (MAC), and it is a normalized LAC per unit density of a substance that produces a constant result for a particular element or substance (i.e., independent of the density of the material).

$$\frac{\mu}{\rho} = t^{-1} \ln\left(\frac{I_o}{I}\right) \tag{2}$$

The μ/ρ for a mixture and composite can be determined theoretically by the following relation:

$$\mu_m = \frac{\mu}{\rho} = \sum w_i \left(\frac{\mu}{\rho}\right)_i \tag{3}$$

Here, $W_i = (n_i A_i / \Sigma_j n_i A_j)$ is a weight fraction; A_i and n_i are the ith element's atomic weight and number of formula units, respectively.

$$\mu = ln\frac{\left(\frac{I_o}{I_t}\right)}{t} \tag{4}$$

where I_t is the intensity at a depth of t cm. The LAC increases with increasing physical density and the atomic number of the absorbing material.

3.2. Half-value layer and tenth-value layer

The HVL is the most common quantitative parameter for describing the materials' attenuation ability. The HVL and TVL indicate the material thickness required to reduce radiation dose by one-half and one-tenth of the initial dose, respectively. The formulae below describe the HVL and TVL values with the μ.

$$\text{HVL} = X_h = \frac{\ln 2}{\mu} \tag{5}$$

$$\text{TVL} = X_h = \frac{\ln 10}{\mu} \tag{6}$$

The quantity of radiation that travels through a particular thickness of material is determined by the energy of individual photons along with materials atomic number (Z) and the density (ρ)

The mean distance between two subsequent contacts of the photon as it travels through the materials, and it is derived by LAC, The MFP is:

$$\text{MFP} = \frac{\int_0^\infty x \, e^{-\mu x} \, \mathrm{dx}}{\int_0^\infty e^{-\mu x} \, \mathrm{dx}} = \frac{1}{\mu} \tag{7}$$

The energy distribution of the particles about the medium and the density affects the MFP.

3.3. Effective atomic number (Z_{eff}), electron density (N_{eff}), and conductivity (C_{eff})

The Z_{eff} is the percentage of total electrons in a sample that interacts with photons. It is calculated by dividing the total atomic cross-section (σ_a) by total electronic cross-section values (σ_e) [18].

$$Z_{\text{eff}} = \frac{\sigma_a}{\sigma_e} = \frac{\sum_i f_i A_i \left(\frac{\mu}{\rho}\right)_i}{\sum_j \frac{A_j}{Z_j} \left(\frac{\mu}{\rho}\right)_j} \tag{8}$$

Here, $\sigma_a = \frac{1}{N_A} \sum_i f_i A_i \left(\frac{\mu}{\rho}\right)_i$ and $\sigma_e = \frac{1}{N_A} \sum_i \frac{f_i A_i}{Z_i} \left(\frac{\mu}{\rho}\right)_i$, where N_A and f_i are the Avogadro's number and fractional abundance, respectively. The N_{eff} refers to the number of electrons per unit mass, and it is closely related to Equation (7). The N_{eff} per unit volume of the material can be calculated using mass attenuation coefficient (μ_m) and electronic cross-section (σ_e) [18]:

$$N_{\text{eff}} = \frac{\mu_m}{\sigma_e} = \frac{N_A}{M} Z_{eff} \sum_i n_i \tag{9}$$

where μ_m and $\Sigma_i n_i = n$ are the average atomic weight and the total number of atoms. The C_{eff} is the samples' effective conductivity, which is measured in (S/m). C_{eff} is proportional to N_{eff} and can be calculated as follows:

$$C_{eff} = \left(\frac{N_{eff} \, \rho e^2 \tau}{m_e}\right) 10^3 \tag{10}$$

where $\tau = (h/2\pi K_B T)$ is the average relaxation time.

3.4. Buildup factor and neutron removal cross-section Σ_R

EBF is a concept derived from secondary particles, which are primarily associated with Compton scattering (CS). The interpolation method for the equivalent atomic number (Z_{eq}) can be used to calculate the EBF, as given in below [19]:

$$Z_{eq} = \frac{Z_1(\log R_2 - \log R) + Z_2 (\log R - \log R_1)}{(\log R_2 - \log R_1)} \tag{11}$$

where $R = (\mu_m)_{\text{Compt}}/(\mu_m)_{\text{total}}$ for a given glass, Z_1 and Z_2 are connected to the ratio R_1 and R_2, respectively. For the evaluation of photon buildup parameters, the G-P fitting method includes five fitting parameters, b, c, a, X_k, and d, which are dependent on Z_{eq} and photon density. The following logarithmic interpolation formula is often used to interpret the G-P fitting coefficient:

$$P = \frac{P_1 \left(\log Z_2 - \log Z_{eq}\right) + P_2 \left(\log Z_{eq} - \log Z_1\right)}{(\log Z_2 - \log Z_1)} \tag{12}$$

where P_1 and P_2 designate the G-P fitting parameters. The following formulae can be used to calculate EBF values.

$$B(E, X) = 1 + \frac{b-1}{K-1}(K^x - 1) \text{ for K} \neq 1 \tag{13}$$

Table 2
γ-ray/neutron shielding parameters formulae with unit

Shielding parameters	Formula	Unit
Mass attenuation coefficient (MAC)	μ_m (or) $\frac{\mu}{\rho} = t^{-1} \ln\left(\frac{I_o}{I}\right)$	cm^2/g
Linear attenuation coefficient (LAC)	$\mu = \ln\frac{\left(\frac{I_o}{I}\right)}{t}$	cm^{-1}
Half-value layer (HVL)	HVL = $X_h = \frac{\ln 2}{\mu}$	cm
Tenth-value layer (TVL)	TVL = $X_h = \frac{\ln 10}{\mu}$	cm
Total atomic cross-section	$\sigma_a = \frac{1}{N_A} \sum_i f_i A_i \left(\frac{\mu}{\rho}\right)_i$	cm^2/atom
Total electronic cross-section	$\sigma_e = \frac{1}{N_A} \sum_i \frac{f_i A_i}{Z_i} \left(\frac{\mu}{\rho}\right)_i$	cm^2/electron
Effective atomic number	$Z_{eff} = \frac{\sigma_a}{\sigma_e} = \frac{\sum_i f_i A_i \left(\frac{\mu}{\rho}\right)_i}{\sum_j \frac{A_j}{Z_j} \left(\frac{\mu}{\rho}\right)_j}$	–
Effective electron number	$N_{eff} = \frac{\mu_m}{\sigma_e} = \frac{N_A}{M} Z_{eff} \sum_i n_i$	Electrons/g
Effective conductivity	$C_{eff} = \left(\frac{N_{eff}\, \rho e^2 \tau}{m_e}\right) 10^3$	S/m
Equivalent atomic number	$Z_{eq} = \frac{Z_1 (\log R_2 - \log R) + Z_2 (\log R - \log R_1)}{(\log R_2 - \log R_1)}$	–
Neutron removal cross-section Σ_R	$\Sigma_R = \sum_i \rho_i (\Sigma_R/\rho)_i$	cm^2/g

$$B(E, X) = 1 + (b - 1)x \text{ for K} = 1 \qquad (14)$$

where $K(E,X) = CX^a + d\, \dfrac{\tanh\left(\frac{x}{X_k} - 2\right) - \tanh(-2)}{1 - \tanh(-2)}$ for x ≤ 40 mfp is the absorbed dose, and E refers to the incident energy.

The generic formula can be used to compute the removal cross-section for substances using the value of $\Sigma_{R/\rho}$ or Σ_R for different elements in the mixture and composites:

$$\Sigma_R = \sum_i \rho_i (\Sigma_R/\rho)_i \qquad (15)$$

For a material sample with *m* substances, the removal cross-section Σ_{R_s} (cm^{-1}) will be:

$$\Sigma_{R_s} = \sum_{X=1}^{m} \rho_X \left(\sum_R /\rho\right)_X \qquad (16)$$

Table 2 illustrates the various shielding parameters of the studied glasses utilized by the Phy-X software program.

4. Results and Discussion

Radiation shielding characteristics for RE co-doped borate, phosphate, and silicate glass systems (G1–G10) were estimated using Phy-X/PSD software in the energy range of 1 KeV to 100 GeV. Figure 1 depicts the relationship between incident γ-photon energy and μ_m, as well as photon interaction with all glass samples in various energy regions (Photoelectric absorption (PEA), CS, and pair production (PP) in the electronic and nuclear fields). The μ_m values are considered to be influenced by thermal, chemical, and molecular structure. The first layer that the radiation beam encounters attenuates considerably more photons than subsequent layers, resulting in an attenuation decrease as a function of photon energy. The μ_m of all glasses decreases as the photon energy increases, and discontinuities occurred at some photon energies that related to the binding energies of the electrons in the different shells of heavy elements such as Ce^{3+}, Dy^{3+}, Sm^{3+}, Pr^{3+}, Eu^{2+}, and Nd^{3+} ions. When the energy of the γ-rays is only above the binding energy of the innermost electron shell, such as the K-shell of the atoms interacting with photons, the K-edge suddenly increases in γ-ray absorption. Physically, PEA of photons causes this abrupt rise in attenuation. As a result, strong peaks appear when photoelectric interaction occurs at specific energies, indicating the presence of two attenuation factors at the same energy. These peaks become more apparent at the binding energy for elements with a relatively high atomic number (rare earths). The μ_m value of G3, G4, and G6 glasses has a unique pattern due to the presence of *L*- and *K*-absorption edges in Ce^{3+} ions.

Figure 1
Mass attenuation coefficient (*μ/ρ*) of rare earth co-doped glasses (G1–G10) as a function of photon energy range 1 KeV–100 GeV
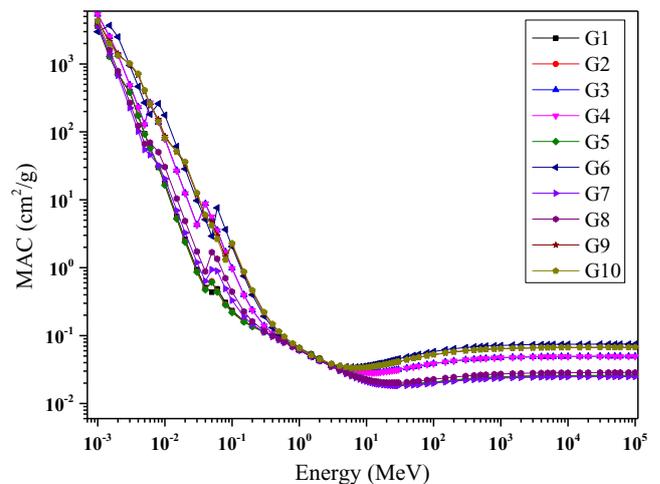

In an energy region of 0.1 to 1 MeV, the values of the attenuation coefficient were nearly consistent. This is because in this energy zone, the CS dominates, which is independent of atomic number (Z). The photon energy increases above 10 MeV, and the influence

of CS rapidly faded because PP became the dominant mechanism and it is related to Z^2. The PEA is preferred in medical applications because it is dependent on the atomic number of the absorbing material, whereas the CS is dependent on the electron density [20]. The Compton Effect is less dependent on the atomic number of the substance than the photoelectric effect. As a result, as the amount of B_2O_3 in the zone dominated by the PEA increases, the μ_m value decreases in G7 and G8 glasses. Because the G6, G9, and G10 glasses have a high Z and ρ, they respond to the PP more in the higher energy region, resulting in a relatively high μ_m. The LAC (μ) values (Figure 2) of all the glass samples followed nearly identical patterns as μ_m values vs. photon energy.

Figure 2
Linear attenuation coefficient (μ) of rare earth co-doped glasses (G1–G10) as a function of photon energy range 1 KeV–100 GeV
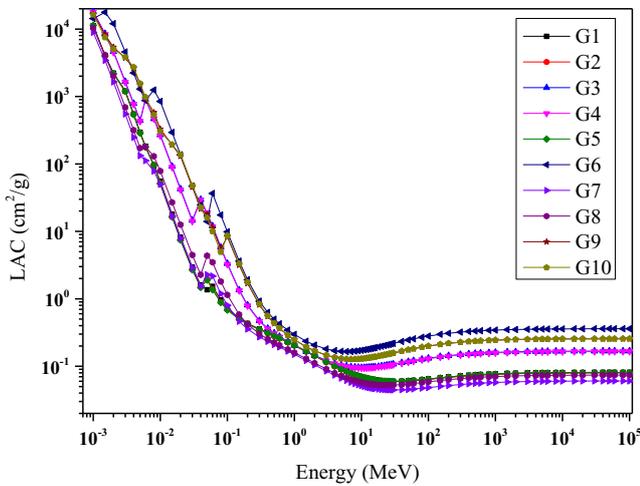
According to the Equations (7) and (8), the HVL and TVL values associated with MFP are all identical and proportionate. Figure 3 (a) and (b) illustrate the variation in HVL and TVL of all

the glass samples. HVL has the exact opposite of attenuation coefficient values in terms of energy dependence. With increased photon energy, the attenuation coefficient declines quickly, causing the penetrating ability to increase. As a result, HVL values for all glasses have increased as the acceleration decreases as the energy increases. It is discovered that the energy of a mono-energetic beam of γ-photons with the same penetrating ability as the spectrum of photons reaches its highest value at a certain energy point known as effective energy, where the HVL gets the highest value (Figure 3(a)). Furthermore, γ-photon penetration diminishes as energy increases, resulting in a saturation of the HVL value for all glasses.

In addition to HVL values, TVL is a factor that specifies the material thickness needed to lower the incoming γ-photon energy to $(1/10)^{th}$ of the original value. It is particularly useful in medical radiation applications. Figure 3(b) depicts the variability in TVL values as a function of incident γ-photon energy. Their changes are identical to the HVL values in terms of energy and material compositions. The density of the material has a significant impact on the MFP of γ-photon penetration through it. The energy of photons influences their probability of interacting, particularly with the photoelectric effect. As the photon energy increases, the probability of interactions decreases and the MFP increases as a result, as shown in Figure 4.

In the low-energy zone where the PEA is dominant, HVL, TVL, and MFP values are lowest and increase as incident photon energy increases. Glasses with high transparency, high mechanical strength, high melting point, and good homogeneity, as well as compositions of elements with a high atomic number, are chosen for radiation shielding applications, taking into account the low HVL, TVL, and MFP values [18]. The presence of Ba^{2+} heavy metal ion in certain glass compositions, together with Al^{2+} ion as a strengthening agent in host elements, leads to high density. The low HVL, TVL, and MAC were explored by relatively high-density glasses such as G6, G9, G10, G4, and G3, whereas the low-density and the highest B_2O_3 content glasses G7 and G8 had larger values of these parameters. Low HVL materials are recommended for low cost in shielding applications since a lower HVL value equals a thinner material that halves the penetrating photon flux. The glasses G7 and

Figure 3
(a) Half-value layer of the rare earth co-doped glasses (G1–G10) as a function of photon energy range 1 KeV–100 GeV and (b) tenth-value layer of the rare earth co-doped glasses (G1–G10) as a function of photon energy range 1 KeV–100 GeV
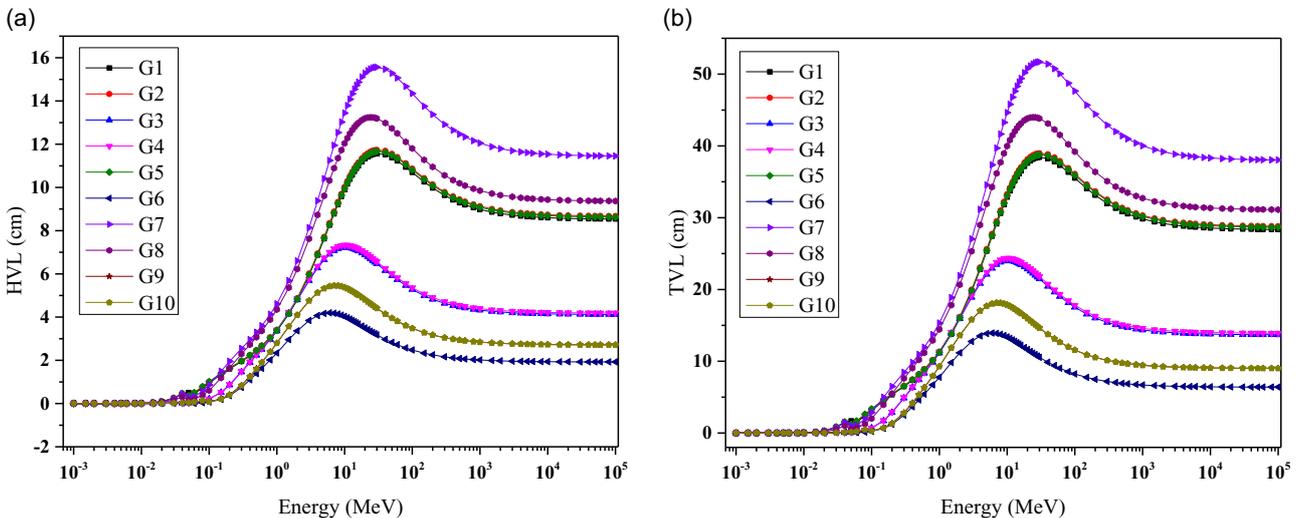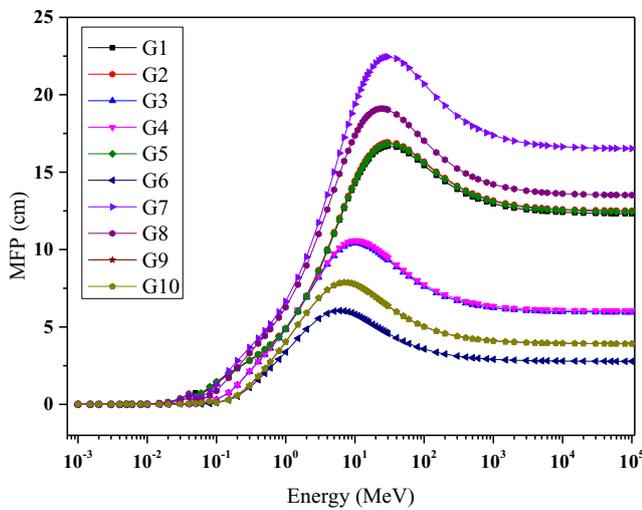
Figure 4
Mean free path of the rare earth co-doped glasses (G1–G10) as a function of photon energy range 1 KeV–100 GeV

G8 contain the elements, although the increase of mole fraction of Pr^{3+} ion by decrease borate in G8, resulting a lower penetration layer values than G7. The glass sample G6 is preferred for shielding purposes since it has a lower HVL, TVL, and MFP value than the other studied glasses, even though the MFP findings of the studied glasses were identical. The reason for the lower HVL could be due to its very high density when compared with other glasses taken in this study. The HVL of Pb, ordinary concrete, and G6 at 15 MeV is 1.08, 13.9 [21], and 2.8 cm respectively. Table 3 shows the maximum values of HVL, TVL, and MFP corresponding to the effective energies of all the glasses.

Table 3
The maximum value of HVL, TVL, and MFP associated with their effective energy of all glasses

Sample code	Effective energy (MeV)	HVL (cm)	TVL (cm)	MFP (cm)
G1	25.90	11.58	38.51	16.80
G2	25.90	11.58	38.51	16.80
G3	10.37	7.241	24.13	10.54
G4	10.37	7.241	24.13	10.54
G5	25.90	11.58	38.51	16.80
G6	**6.61**	**4.914**	**6.73**	**6.04**
G7	25.90	15.50	53.13	22.43
G8	25.90	13.19	43.92	19.18
G9	6.61	5.44	18.08	7.83
G10	6.61	5.44	18.08	7.83

Figures 5 and 6 illustrate the variation of Z_{eff} and N_{eff} with a photon energy range of 1 KeV – 100 GeV for all glass samples (G1–G10), respectively. The Z_{eff} decreases as photon energy increases, which is because high-energy photons can travel deeper into the absorber material without interaction. The γ-photon attenuation ability of the absorbent material is reflected in the magnitude of the Z_{eff} value. Photons are highly attenuated in these materials because elementals with high Z_{eff} values are the chosen targets for more photon collisions. Since Equation (9) relates these two parameters, it can be seen from these graphs that the variations

of Z_{eff} and N_{eff} with photon energy are nearly identical. The Z_{eff} and N_{eff} are a metric that can be used to predict the ionizing radiation response of different elemental configurations. At the lower energy band, all glasses have two peaks traced in both Z_{eff} and N_{eff}. When photon energy is near the L- and K-absorption edges of the elements (Ce, Dy, Sm, Pr, Eu, and Nd) contained in the glasses, there are abrupt changes in Z_{eff} and N_{eff} values due to the jump in μ_m values at the L- and K-absorption edges of the elements.

Figure 5
Effective atomic number (Z_{eff}) of the rare earth co-doped glasses (G1–G10) as a function of photon energy
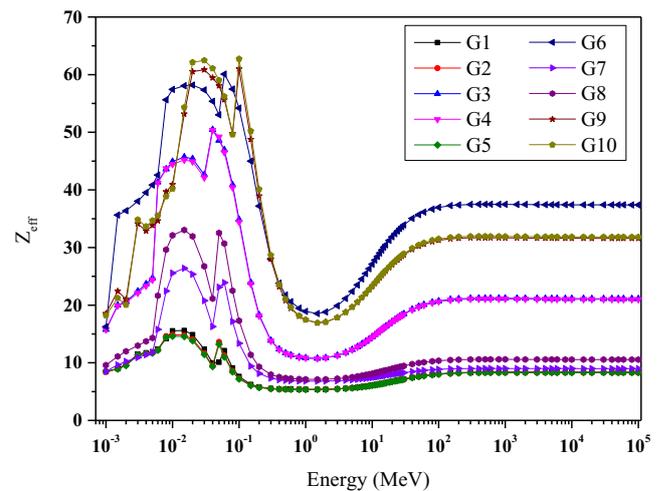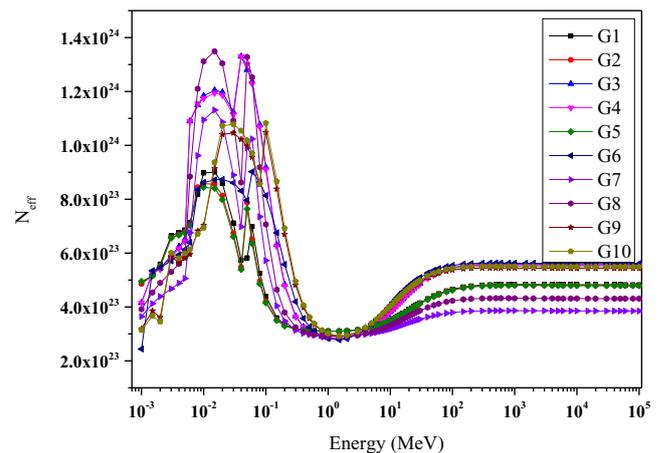

Figure 6
Effective electron density (N_{eff}) of the rare earth co-doped glasses (G1–G10) as a function of photon energy

The photon energy dependence of total atomic cross-section (σ_a) and electron cross-section (σ_e) is prominent only at low energies, resulting in high responses of both Z_{eff} and N_{eff} to the energy region. As a result, several partial photon-interaction mechanisms are accurately related to the composing element "Z." These interactions are important in Z_{eff} variation with γ-ray energy, and it is interesting to note that the Z-dependence of the

cross-section for PE absorption, CS, and PP processes are Z^{4-5}, Z, and Z^{2-3}, respectively. Higher atomic number absorbers have a high probability of photoelectric interactions in low-energy regions (< 0.1 MeV). The PEA edges of Pb and Ba are associated with irregular jumps in Z_{eff} and N_{eff} values. At energies where the CS progressively emerges as the dominant interaction process (about 0.4–4 MeV), the N_{eff} values are remarkably independent of the atomic number of the constituting elements. Bagheri and Adeli [22] reported that increasing Bi_2O_3, PbO, and BaO in glasses improves their σ_a values. The results are in good accord with the present investigation, with the BaO-containing G6 glass and the Pb-containing G9/G10 glasses having higher Z_{eff} values in the low-energy zone than the other glasses.

There is a distinct variation in Z_{eff} values of all the studied glasses in the entire energy zone, revealing that the value depends on their atomic number (Figure 5). But, the N_{eff} values of all the studied glasses are nearly identical in the intermediate energy zone, indicating that the CS dominates in the intermediate energy zone irrespective of atomic number (Figure 6).

Furthermore, the photon with energies ranging from 0.0015 to 1 GeV was used to calculate the effective electron conductivity (C_{eff}) values of the tested glass samples. Figure 7 depicts the change in effective conductivity for all glass samples at 300 K. The C_{eff} parameter is directly proportional to the material densities and the effective electron numbers. At a low-energy band, the C_{eff} value has reached its maximum value in all the glasses, where the photoelectric effect is prevalent. The C_{eff} values of all the glasses have nearly flattened out in an intermediate zone, where the CS dominates.

Figure 7
Effective electron conductivity (C_{eff}) of the rare earth co-doped glasses (G1–G10) as a function of photon energy
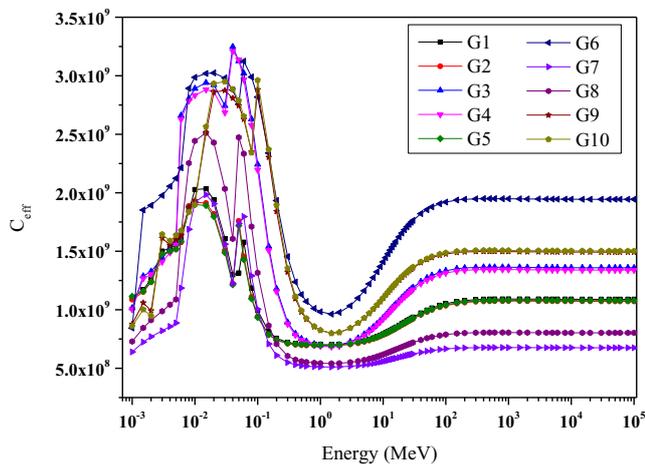

Figure 8 depicts the energy-dependent variations in equivalent atomic number (Z_{eq}) values acquired for the glasses studied. It is observed that there are three separate Z_{eq} variation energy bands, with PEA, CS, and PP dominating in the energy range (0.015–0.03 MeV), (0.03–1 MeV), and above 1 MeV, respectively. The fact that the Z_{eq} of all the glasses in the intermediate energy zone is relatively high, suggests that the process is more scattering than energy absorption and PP. At low energy, the Z_{eq} of G10 and

G9 is lower than that of G6, but in the intermediate energy band, the value of these glasses exceeds that of G6 glass. The higher Z_{eq} values of G10 and G9 glasses in an energy band (0.03–1 MeV) relative to the other examined glasses are attributable to the fact that these glasses contain Pb ions, which scattered γ-photons more than other glasses. The density of G7 and G8 glasses decreases while B_2O_3 (boron oxide) concentration increases, however, it is higher than H_3BO_3 (Boric acid) doped G1, G2, and G5 glasses. Because G7 and G8 glasses have a high viscosity and a large extension area during casting, their thickness as well as Z_{eq} are greater than those of G1, G2, and G5.

Figure 8
Equivalent atomic number (Z_{eq}) of the rare earth co-doped glasses (G1–G10) as a function of photon energy in the range 0.015 MeV–15 MeV
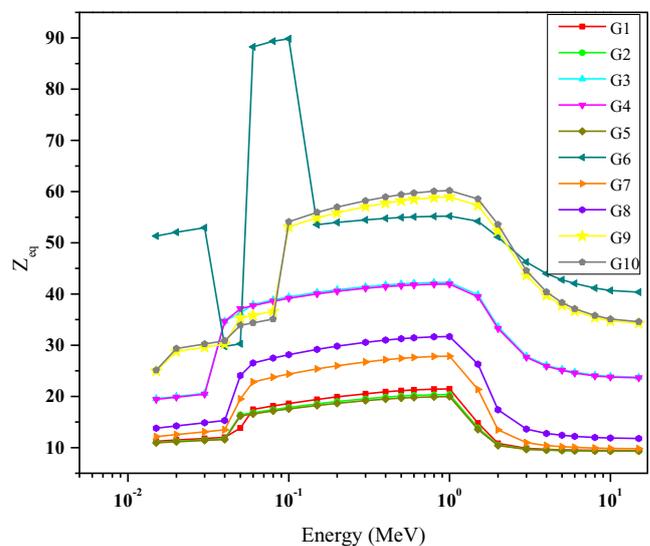

4.1. Energy dependence EBF/EABF

EBF/EABF were calculated for each glass sample, Figures 9 (a)–(d) and 10 (a)–(d) illustrate the variation of EBFs and EABFs of all the studied glasses (G1–G10) with photon energy range 0.015–15 MeV at specified penetration depths of 1, 10, 20, and 40 mfp, respectively. These figures show that the buildup factors vary in three different zones depending on the photon-material interaction. All the glasses' EBF and EABF values were found to be lowest in the lower and higher energy zones where PEA and PP dominate respectively, and highest in the intermediate energy zone (CS dominates). Above the photon energy (> 1 MeV), the concentration of e^-–e^+ particles may cause the secondary γ-ray photon to be initiated by the destruction of the e^+ with the e^- at rest, resulting in significant increases in the photon intensity.

The rapid rise in PEA of γ-ray photons detected just above the binding energy of the atom's K-shell electrons is known as the K-absorption edge. As illustrated in Figures 9 (a)–(d) and 10 (a)–(d), a large intensive peak in the EBF and EABF values of G6 glass at 1 mfp was detected at 0.0304 MeV energy, which could be attributable to K-edge of Sb absorption. In addition, at the low-energy region, a peak in buildup factors at 0.040 MeV, 0.048 MeV, and 0.041 MeV is due to the K-edge of Ce, Eu, and Pr elements, which are present in (G1, G2, G3, and G4), (G9 and

Figure 9

Exposure buildup factor (EBF) of the rare earth co-doped glasses (G1–G10) as a function of photon energy in the range 0.015 MeV–15 MeV for (a) 1 MFP, (b) 10 MFP, (c) 20 MFP and (d) 40 MFP
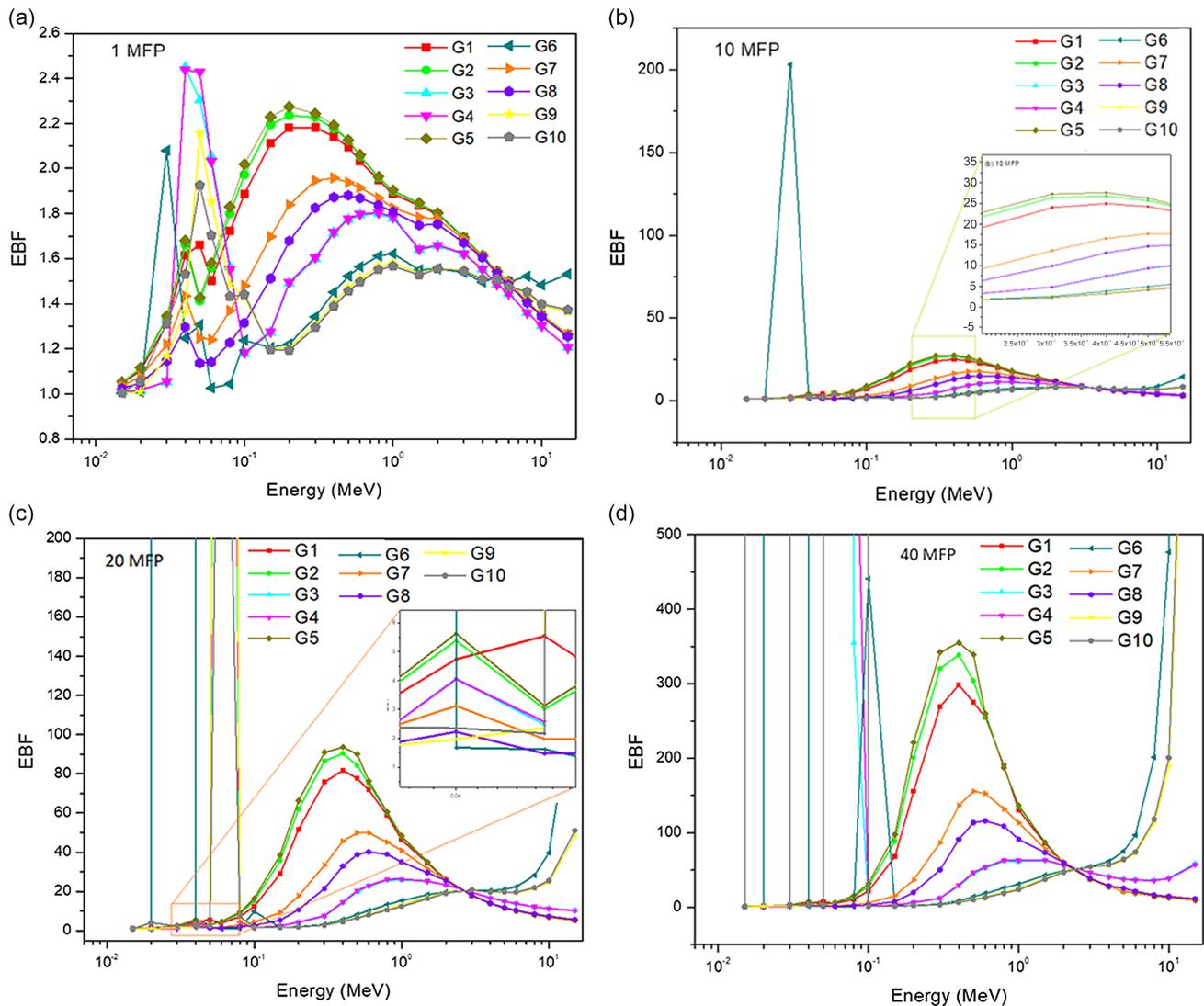
G10) and (G5, G7, and G8) glasses respectively [23]. The EBF and EABF, peak at 0.193 MeV in G5, G2, and G1, at 0.39 MeV in G7 and G8, at 0.779 MeV in G3 and G4, and 0.988 MeV in G6, G9 and G10 at 1 mfp (Figures 9(a) and 10(a)). For all of the selected penetration depths (1, 10, 20, and 40 MFP), the highest values were obtained for the G5, G2, and G1glass, while the lowest values were observed for the G9, G10, and G6. Specifically, G5 glass has relatively higher buildup factor values than the other studied glasses in an intermediate energy zone for all mfps. The variation of EBF and EABF associated with the incident photon energy reached high values for 40 mfp (Figures 9(d) and 10(d)).

### 4.2. Penetration depth dependence of EBF/EABF

Figures 11 (a)–(d) and 12 (a)–(d) show the variation of EBF and EABF with MFPs at various incident photon energies (0.015, 0.15, 1.5, and 15 MeV). As the penetration depths increase, the

buildup factor values of the glasses increase as well. The buildup factor values differ depending on the chemical composition of the glasses at this specific energy. At the lowest energy such as 0.015 MeV (Figures 11(a) and 12(a)), except for G6 and G10 glasses, the EBF and EABF values exponentially increase. These values are lower than those of other glasses and are nearly constant after 10 mfp for G6 and G10 glasses. One intriguing observation is that the EBF values of the G3 and G4 glasses increase after 30 mfp (Figure 11(a)), indicating that the high Ba ion content in these glasses generated more non-bonding oxygen, allowing photon energy to penetrate more distance to them.

At 0.15 MeV (Figures 11(b) and 12(b)), the EBF and EABF values are the smallest and highest for (G6, G9, and G10) and (G5, G2, and G1) glasses in the penetration depth range 0–40 mfp, respectively. In this energy, the buildup factor values of all the glasses increase linearly over the penetration depths, owing

Figure 10
Energy absorption buildup factor (EABF) of the rare earth co-doped glasses (G1–G10) as a function of photon energy in the range 0.015 MeV–15 MeV for (a) 1 MFP, (b) 10 MFP, (c) 20 MFP and (d) 40 MFP
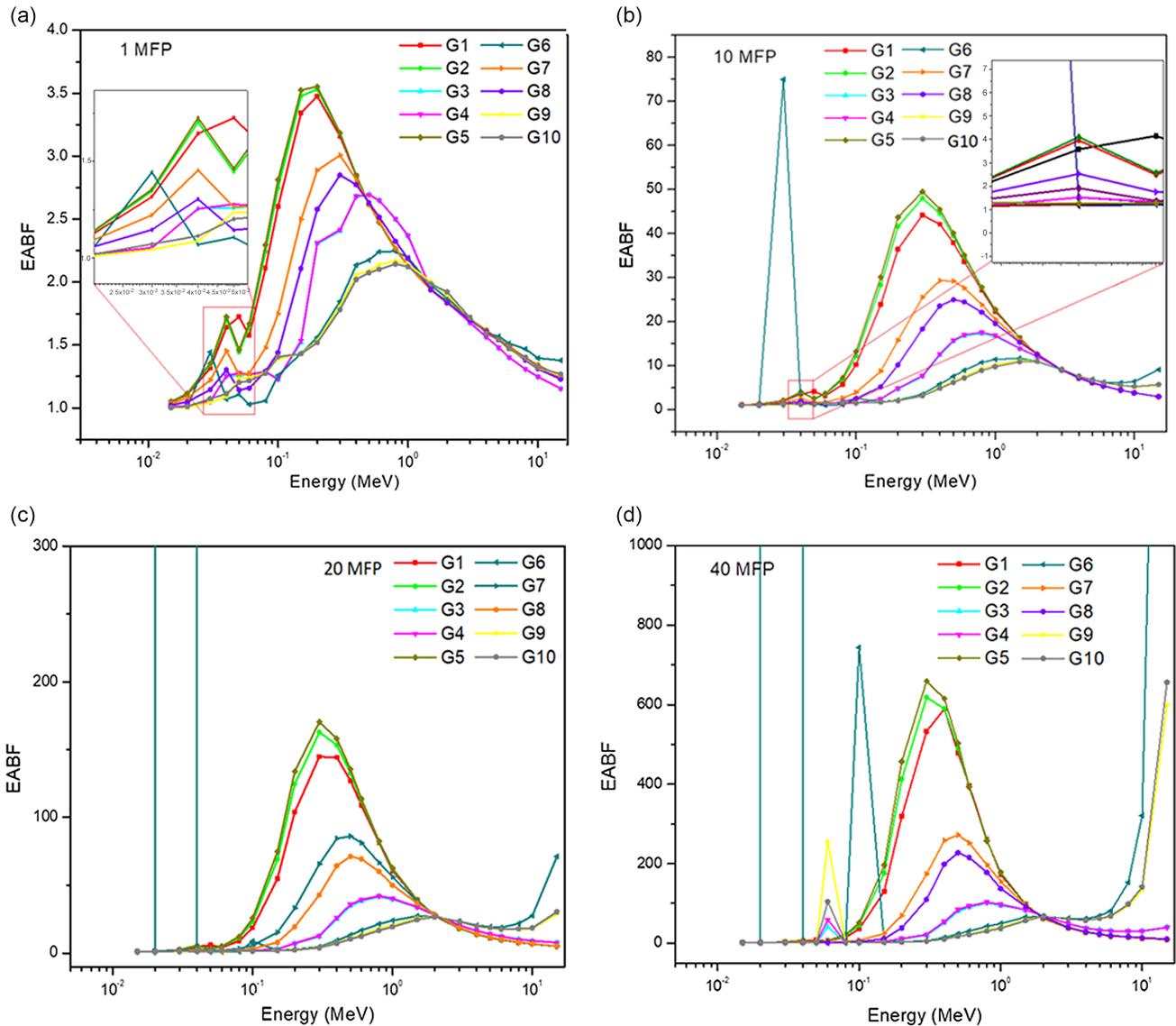
to the intense PEA. At 1.5 MeV, the buildup factors of these glass samples are almost independent of the elemental composition of the glasses due to the CS process. However, the buildup factor values of the G1, G2, and G5 are nearly identical and higher than those of other studied glasses (Figures 11(c) and 12(c)), implying that the incident γ-photon generated more scattering in these glasses.

At 15 MeV, both buildup factors for the given penetration range attain their maximum values (Figures 11(d) and 12(d)). This could be because PP dominates, causing Z_{eq} dependency. Specifically, G6 glass has the highest buildup factor values in this energy zone due to its highest Z_{eq} (89.83 $< Z_{eq} <$ 40.36). This is because the PP process has taken over, resulting in an $e^- - e^+$ pair with a lower penetration depth. After some collisions within the glass samples, the $e^- - e^+$ emitted in the process

slowed down and went through an annihilation process, producing two γ-photons (511 KeV) in opposite directions [24, 25]. As a result, rather than absorbing high-energy photons (over 10 MeV), the pair production and annihilation processes twice the photons. As a consequence, EBF and EABF values are proportional to Z_{eq}, with maximum EBF/EABF values seen for G6 ((Z_{eq})$_{high}$ glass) and lowest EBF values observed for G5 ((Z_{eq})$_{low}$ glass).

To evaluate the weakening of fast neutrons within the studied glasses, the term effective removal cross-section Σ_R is utilized. It is well known that glass with a high Σ_R value provides excellent neutron protection [26]. Secondary photons are generated by neutron attenuation due to inelastic scattering interactions with nuclei, requiring the use of both low and high Z elements in

Figure 11

Exposure buildup factor (EBF) of the rare earth co-doped glasses (G1–G10) as a function of penetration depth in the range 0.5–40 mfp for (a) 0.015 MeV, (b) 0.15 MeV, (c) 1.5 MeV and (d) 15 MeV
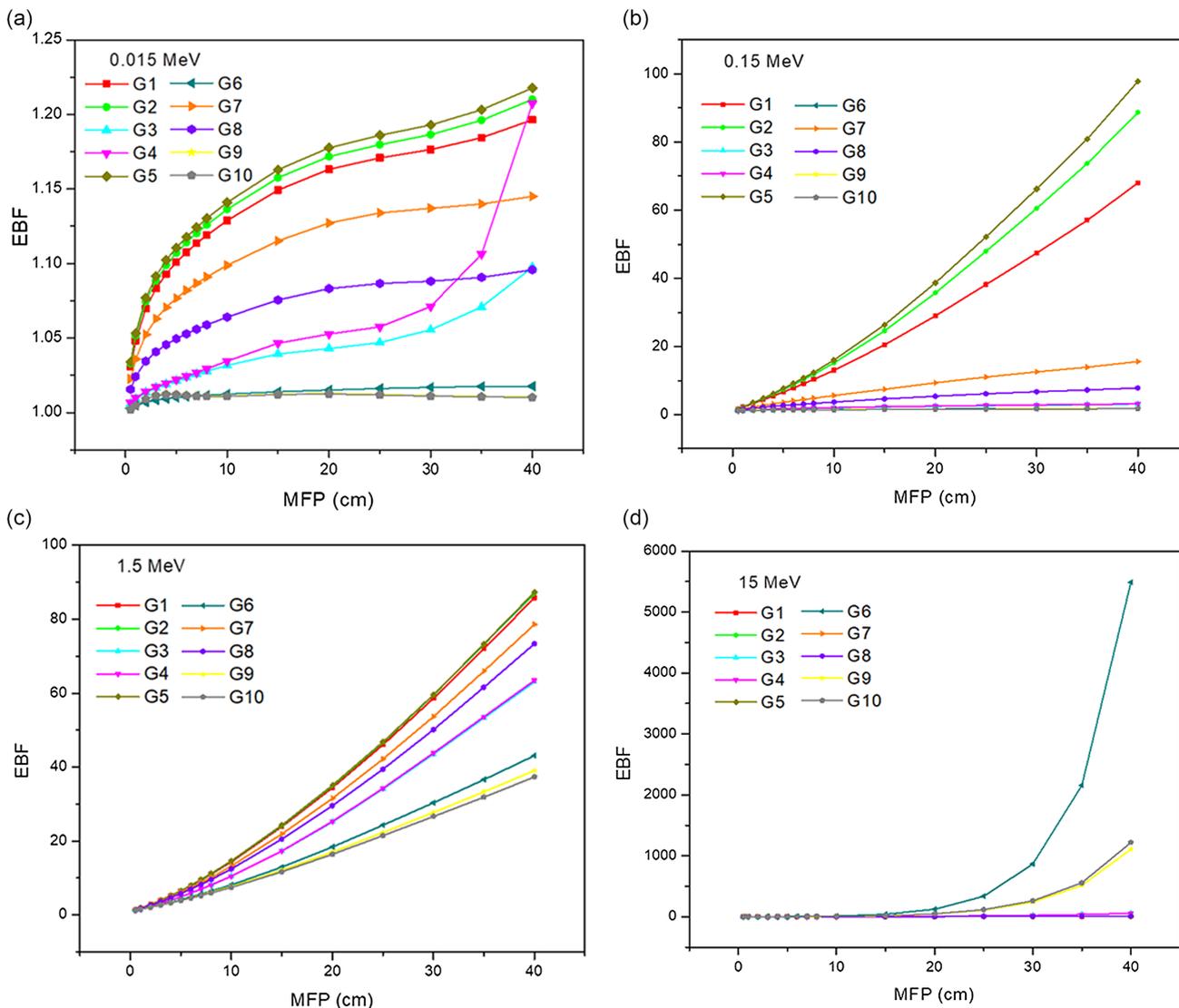

Table 4

Comparison of fast neutron removal cross-section (Σ_R) co-doped rare earth glasses (G1–G10) with conventional neutron shielding materials

Sample code	Σ_R (cm^{-1})	Ref. No
G1	0.193	Present study
G2	0.191	
G3	0.106	
G4	0.105	
G5	0.192	
G6	0.104	
G7	0.110	
G8	0.113	
G9	0.091	
G10	0.091	
Water	0.102	[27]
Ordinary concrete (OC)	0.093	[27]
Hematite-serpentine concrete (HSC)	0.097	[27]
Graphite	0.077	[28]

neutron shielding glasses. Equation (15) was used to calculate the fast neutron cross-section (Σ_R) for all of the glasses studied. Figure 13 compares the Σ_R of the studies glasses to the Σ_R of various regularly employed neutron shielding materials like water, ordinary concrete (OC), Hematite-serpentine concrete (HSC), and graphite, their values are given in Table 4. The removal cross-section was found to be highest for G1, G5, and G2 glasses, with values of 0.193, 0.192, and 0.191, respectively, and lowest for the other glasses, with values ranging from 0.092 to 0.113. High quantities of B_2O_3 are present in the G7 and G8 glasses, lowering the Σ_R value substantially. This is because the lower atomic number B element substitutes for the higher atomic number Dy and Pr atoms in the glasses. When compared to commonly used neutron shielding materials, it is obvious that some of our studied glasses (G1, G5, and G2) are promising prospects for neutron shielding applications. As a result, the highest H_3BO_3 contribution gives the best neutron shielding, showing that decreasing the atomic number supports neutron attenuation.

Figure 12
Energy absorption buildup factor (EABF) of the rare earth co-doped glasses (G1–G10) as a function of penetration depth in the range 0.5–40 mfp for (a) 0.015 MeV, (b) 0.15 MeV, (c) 1.5 MeV and (d) 15 MeV
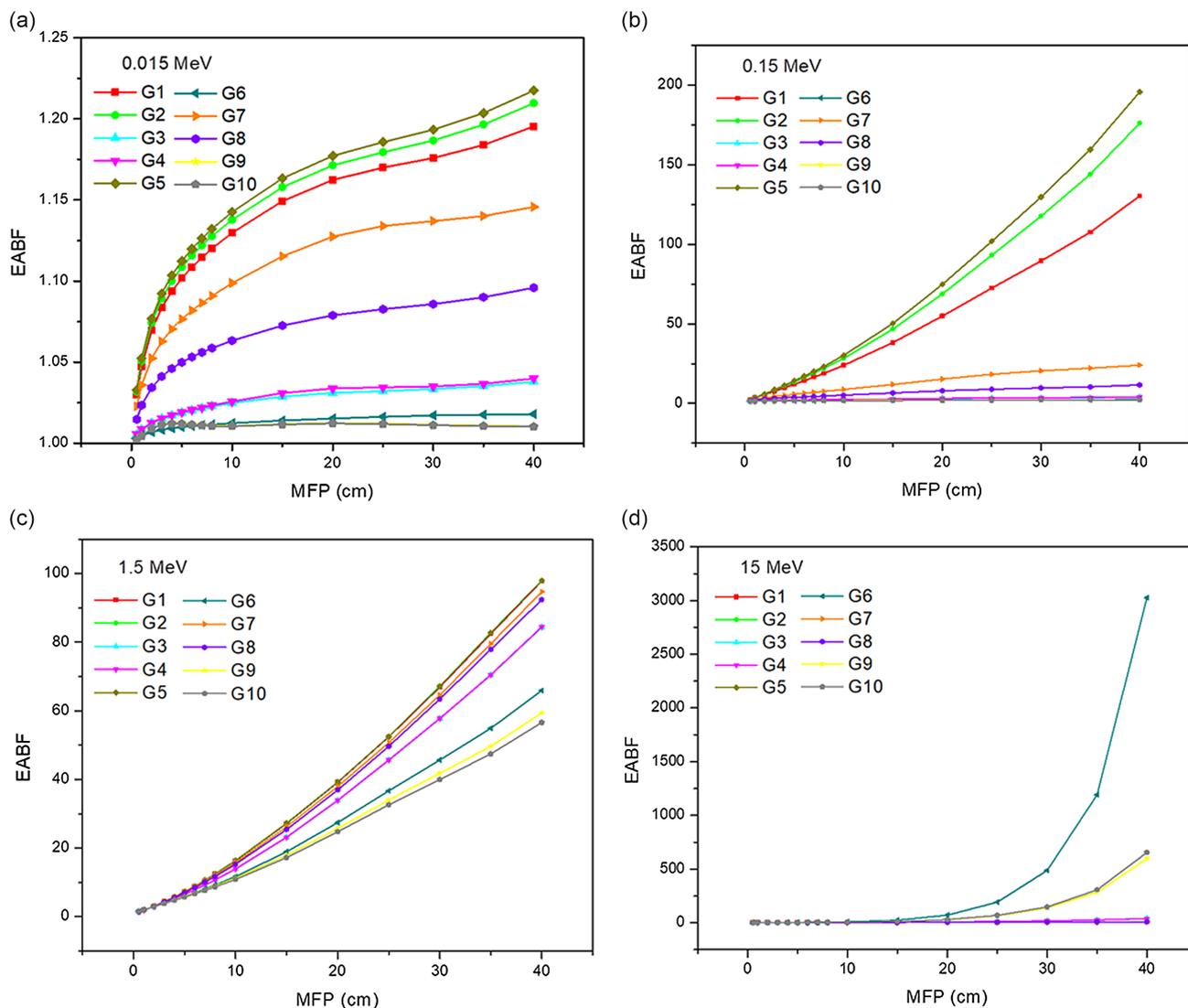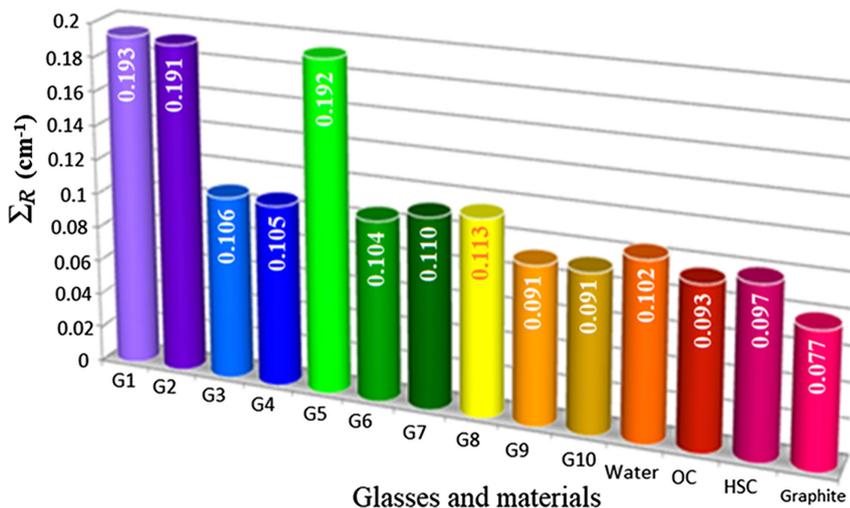

Figure 13
Fast removal cross-section of the rare earth co-doped glasses (G1–G10) with the conventional neutron shielding materials

5. Conclusion

The high density and Z_{eq} of G6 glass exhibit low buildup factor values spanning the 0.5 to 40 mfp range, with energy values of 0.015, 0.15, and 1.5 MeV. Hence, the values of the glass turned high at 15 MeV, indicating that the incident γ-photon generated a greater number of electron-positron pairs in the glass. The results show that HVL and TVL can be sorted in the following order for all glasses: G7 > G8 > G1/G2/G5 > G3/G4 > G9/G10 > G6. The maximum values of HVL, TVL, and MFP of G6 glass were found to be 6.13 cm, 6.54 cm, and 6.36 cm, respectively. HVL results compared to conventional materials show that G6 glass can attenuate 15 MeV photons at one-fourth thickness required for ordinary concrete to attenuate. The G6, G9, and G10 glasses had the highest Z_{eff} and N_{eff} values than the other studied glasses. The highest C_{eff} values are found in G6 glass, whereas the lowest C_{eff} values are found in G7 glass. The high content of B_2O_3 in G7 and G8 glasses increases HVL, TVL, and MFP values while lowering Z_{eff}, N_{eff}, and C_{eff}. The K-absorption edge of Ce (in G1, G2, G3, G4, and G6), Eu (in G9, G10), Sb (in G6), and Pr (in G5, G6, and G7) elements were found to be at 0.040, 0.048, 0.0304 and 0.041 MeV, respectively, at the lower energy zone. The stepwise variation in Z_{eq} of all the investigated glasses revealed three distinct zones associated with PEA, CS, and PP. In addition, G10, G9, and G6 glasses have a higher Z_{eq} in the intermediate energy zone resulting in increased scattering by photon collision in this region. Due to their larger Z_{eq} values and lower exposure and energy absorption buildup factor values, the Ce^{3+}/Tb^{3+} co-doped GBS scintillating (G6), Eu^{2+}/Nd^{3+} co-doped silicate (G9 and G10) glasses had superior γ-ray shielding performance among the studied glasses. In addition, G1, G5, and G2 glasses have a greater mass removal cross-section than the other investigated glasses, including conventional materials, and hence have potential uses for neutron shielding. As a result, high Z_{eq} elements composition and density play an important role in γ and neutron shielding abilities.

Ethical Statement

This study does not contain any studies with human or animal subjects performed by any of the authors.

Conflicts of Interest

The authors declare that they have no conflicts of interest to this work.

Data Availability Statement

Data sharing does not apply to this article as no new data were created or analyzed in this study. All data are provided already as Tables and Figures.

Author Contribution Statement

Murugasen Priya: Conceptualization, Methodology, Writing – review & editing, Supervision, Project administration, Funding acquisition. **A. Antony Suresh:** Software, Formal analysis. **M. Dhavamurthy:** Validation, Writing – original draft. **A. V. Deepa:** Resources.

References

[1] Kavaz, E., Tekin, H. O., Kilic, G., & Susoy, G. (2020). Newly developed Zinc-Tellurite glass system: An experimental investigation on impact of Ta_2O_5 on nuclear radiation shielding ability. *Journal of Non-Crystalline Solids*, *544*, 120169. https://doi.org/10.1016/j.jnoncrysol.2020.120169

[2] Yin, S., Wang, H., Wang, S., Zhang, J., & Zhu, Y. (2022). Effect of B_2O_3 on the radiation shielding performance of telluride lead glass system. *Crystals*, *12*(2), 178. https://doi.org/10.3390/cryst12020178

[3] Kirdsiri, K., Kaewkhao, J., Chanthima, N., & Limsuwan, P. (2011). Comparative study of silicate glasses containing Bi_2O_3, PbO and BaO: Radiation shielding and optical properties. *Annals of Nuclear Energy*, *38*(6), 1438–1441. https://doi.org/10.1016/j.anucene.2011.01.031

[4] Vani, P., Vinitha, G., Sayyed, M. I., Elbashir, B. O., & Manikandan, N. (2019). Investigation on structural, optical, thermal and gamma photon shielding properties of zinc and barium doped fluorotellurite glasses. *Journal of Non-Crystalline Solids*, *511,* 194–200. https://doi.org/10.1016/j.jnoncrysol.2019.02.005

[5] Naseer, K. A., & Marimuthu, K. (2021). The impact of Er/Yb co-doping on the spectroscopic performance of bismuth borophosphate glasses for photonic applications. *Vacuum*, *183,* 109788. https://doi.org/10.1016/j.vacuum.2020.109788

[6] Mhareb, M. H. A. (2020). Physical, optical and shielding features of $Li_2O–B_2O_3–MgO–Er_2O_3$ glasses co-doped of Sm_2O_3. *Applied Physics A*, *126*(1), 71. https://doi.org/10.1007/s00339-019-3262-9

[7] Kaur, P., Singh, D., & Singh, T. (2019). Sm^{3+} and Gd^{3+} co-doped lead phosphate glasses for γ-rays shielding and sensing. *Journal of Luminescence*, *209*, 74–88. https://doi.org/10.1016/j.jlumin.2019.01.019

[8] Rammah, Y. S., Sayyed, M. I., El-Bashir, B. O., Asiri, S. M., & Al-Hadeethi, Y. (2021). Linear optical features and radiation shielding competence of $ZnO–B_2O_3–TeO_2-Eu_2O_3$ glasses: Role of Eu^{3+} ions. *Optical Materials*, *111*, 110525. https://doi.org/10.1016/j.optmat.2020.110525

[9] Vani, P., Vinitha, G., Sayyed, M. I., AlShammari, M. M., & Manikandan, N. (2021). Effect of rare earth dopants on the radiation shielding properties of barium tellurite glasses. *Nuclear Engineering and Technology*, *53*(12), 4106–4113. https://doi.org/10.1016/j.net.2021.06.009

[10] Sallam, O. I., Madbouly, A. M., Elalaily, N. A., & Ezz-Eldin, F. M. (2020). Physical properties and radiation shielding parameters of bismuth borate glasses doped transition metals. *Journal of Alloys and Compounds*, *843*, 156056. https://doi.org/10.1016/j.jallcom.2020.156056

[11] Chanthima, N., Kaewkhao, J., & Limsuwan, P. (2012). Study of photon interactions and shielding properties of silicate glasses containing Bi_2O_3, BaO and PbO in the energy region of 1 keV to 100 GeV. *Annals of Nuclear Energy*, *41*, 119–124. https://doi.org/10.1016/j.anucene.2011.10.021

[12] Kaur, P., Singh, K. J., Thakur, S., Singh, P., & Bajwa, B. S. (2019). Investigation of bismuth borate glass system modified with barium for structural and gamma-ray shielding properties. *Spectrochimica Acta Part A: Molecular and*

Biomolecular Spectroscopy, *206*, 367–377. https://doi.org/10.1016/j.saa.2018.08.038

[13] Murugasen, P., Dhavamurthy, M., Anthoniammal, P., Suresh, A. A., & Mohapatra, M. (2024). Structural, optical, and thermoluminescence characterizations of 1 mol% Dy^{3+}ion-activated fluro boro-phosphate glass for photonic devices. *Spectrochimica Acta Part A: Molecular and Biomolecular Spectroscopy*, *308*, 123757. https://doi.org/10.1016/j.saa.2023.123757

[14] Vinothkumar, P., Dhavamurthy, M., Mohapatra, M., & Murugasen, P. (2021). Structural, optical and thermo-physical characterizations of co-doped Pr^{3+} and Nd^{3+} ions on $BaCO_3$–H_3BO_3 glasses for microelectronic applications. *Bulletin of Materials Science*, *44*(4), 257. https://doi.org/10.1007/s12034-021-02545-9

[15] Xu, P., Fu, Z., Fan, S., Lin, H., Li, C., Yao, G., . . . , & Zeng, F. (2018). Study on the sensitization of Gd^{3+} on Ce^{3+}/Tb^{3+} co-doped GBS scintillating glass. *Journal of Non-Crystalline Solids*, *481*, 441–446. https://doi.org/10.1016/j.jnoncrysol.2017.11.028

[16] Pawar, P. P., Munishwar, S. R., & Gedam, R. S. (2016). Physical and optical properties of Dy^{3+}/Pr^{3+} co-doped lithium borate glasses for W-LED. *Journal of Alloys and Compounds*, *660*, 347–355. https://doi.org/10.1016/j.jallcom.2015.11.087

[17] Manasa, P., Ran, F., Basavapoornima, C., Depuru, S. R., & Jayasankar, C. K. (2020). Optical characteristics of (Eu^{3+}, Nd^{3+}) co-doped lead fluorosilicate glasses for enhanced photonic device applications. *Journal of Luminescence*, *223*, 117210. https://doi.org/10.1016/j.jlumin.2020.117210

[18] Rammah, Y. S., Özpolat, Ö. F., Alım, B., Şakar, E., El-Mallawany, R., & El-Agawany, F. I. (2020). Assessment of gamma-ray attenuation features for La^{+3} co-doped zinc borotellurite glasses. *Radiation Physics and Chemistry*, *176*, 109069. https://doi.org/10.1016/j.radphyschem.2020.109069

[19] Al-Buriahi, M. S., Sriwunkum, C., Arslan, H., Tonguc, B. T., & Bourham, M. A. (2020). Investigation of barium borate glasses for radiation shielding applications. *Applied Physics A*, *126*(1), 68. https://doi.org/10.1007/s00339-019-3254-9

[20] Al-Buriahi, M. S., & Tonguc, B. T. (2020). Mass attenuation coefficients, effective atomic numbers and electron densities of some contrast agents for computed tomography. *Radiation Physics and Chemistry*, *166*, 108507. https://doi.org/10.1016/j.radphyschem.2019.108507

[21] Tekin, H. O., ALMisned, G., Issa, S. A. M., & Zakaly, H. M. H. (2022). A rapid and direct method for half value layer calculations for nuclear safety studies using MCNPX Monte Carlo code. *Nuclear Engineering and Technology*, *54*(9), 3317–3323. https://doi.org/10.1016/j.net.2022.03.037

[22] Bagheri, R., & Adeli, R. (2020). Gamma-ray shielding properties of phosphate glasses containing Bi_2O_3, PbO, and BaO in different rates. *Radiation Physics and Chemistry*, *174*, 108918. https://doi.org/10.1016/j.radphyschem.2020.108918

[23] Bearden, J. A., & Burr, A. F. (1967). Reevaluation of X-ray atomic energy levels. *Reviews of Modern Physics*, *39*(1), 125–142. https://doi.org/10.1103/RevModPhys.39.125

[24] Singh, T., Kaur, A., Sharma, J., & Singh, P. S. (2018). Gamma rays' shielding parameters for some Pb-Cu binary alloys. *Engineering Science and Technology, an International Journal*, *21*(5), 1078–1085. https://doi.org/10.1016/j.jestch.2018.06.012

[25] Kavaz, E., & Yorgun, N. Y. (2018). Gamma ray buildup factors of lithium borate glasses doped with minerals. *Journal of Alloys and Compounds*, *752*, 61–67. https://doi.org/10.1016/j.jallcom.2018.04.106

[26] Issa, S. A. M., Kassab, L. R. P., Susoy, G., Nishimura, M. V. M., da Silva Mattos, G. R., Bordon, C. D. S., & Tekin, H. O. (2020). Fabrication, optical characteristic, and nuclear radiation shielding properties of newly synthesised $PbO–GeO_2$ glasses. *Applied Physics A*, *126*(9), 748. https://doi.org/10.1007/s00339-020-03928-1

[27] Suresh, A. A., Vinothkumar, P., Mohapatra, M., Dhavamurthy, M., & Murugasen, P. (2022). The effect of rare earth on the radiation shielding properties of transparent lead-free Alumino-borophosphate glass system. *Radiation Physics and Chemistry*, *193*, 109941. https://doi.org/10.1016/j.radphyschem.2021.109941

[28] Bashter, I. I. (1997). Calculation of radiation attenuation coefficients for shielding concretes. *Annals of Nuclear Energy*, *24*(17), 1389–1401. https://doi.org/10.1016/S0306-4549(97)00003-0